Acceleration of a Stratified Current over a Sloping Bottom, Driven by an Alongshelf Pressure Gradient*

DAVID C. CHAPMAN+ AND STEVEN J. LENTZ

Woods Hole Oceanographic Institution, Woods Hole, Massachusetts

(Manuscript received 28 April 2004, in final form 5 December 2004)

ABSTRACT

An idealized theoretical model is developed for the acceleration of a two-dimensional, stratified current over a uniformly sloping bottom, driven by an imposed alongshelf pressure gradient and taking into account the effects of buoyancy advection in the bottom boundary layer. Both downwelling and upwelling pressure gradients are considered. For a specified pressure gradient, the model response depends primarily on the Burger number $S = N\alpha/f$, where N is the initial buoyancy frequency, α is the bottom slope, and f is the Coriolis parameter. Without stratification ($S = 0$), buoyancy advection is absent, and the alongshelf flow accelerates until bottom stress balances the imposed pressure gradient. The e-folding time scale to reach this steady state is the friction time, h/r, where h is the water depth and r is a linear bottom friction coefficient. With stratification ($S \neq 0$), buoyancy advection in the bottom boundary layer produces vertical shear, which prevents the bottom stress from becoming large enough to balance the imposed pressure gradient for many friction time scales. Thus, the alongshelf flow continues to accelerate, potentially producing large velocities. The acceleration increases rapidly with increasing S, such that even relatively weak stratification ($S > 0.2$) has a major impact. These results are supported by numerical model calculations.

1. Introduction

The alongshelf pressure gradient has long been identified as an important driving force for subtidal currents over continental shelves, constituting a significant part of the alongshelf momentum balance in many observational studies (Allen and Smith 1981; Hickey 1984; Lentz and Winant 1986; Lentz 1994; Yankovsky and Garvine 1998; Lentz et al. 1999; to name a few). Among many dynamical applications, the alongshelf pressure gradient plays a critical role in the propagation of coastally trapped waves (e.g., Brink 1991), has been invoked to account for the observed cross-shelf circulation in some coastal upwelling regions (e.g., Smith 1981), has been inferred as the driving mechanism for the mean flow on the Middle Atlantic Bight shelf (e.g., Scott and Csanady 1976; Beardsley and Winant 1979), and has been linked to flow reversals following the relaxation of upwelling winds (e.g., Gan and Allen 2002).

Our understanding of the details of how an alongshelf pressure gradient accelerates a current is based primarily on linear, unstratified flows. That is, a vertically uniform alongshelf pressure gradient (i.e., an alongshelf sea surface slope) accelerates the entire water column until bottom stress becomes large enough to balance the pressure gradient. However, recent developments suggest that this scenario must be modified in the case of a stratified flow over a sloping bottom. As a stratified flow accelerates, the resulting cross-shelf velocity in the bottom boundary layer advects buoyancy laterally, which in turn generates vertical shear in the alongshelf velocity and reduces the flow, and hence stress, at the bottom. This nonlinear process has received considerable attention over the past decade as a mechanism for reducing or eliminating bottom stress and limiting or shutting down cross-shelf transport in the bottom boundary

+ Deceased.

* Woods Hole Oceanographic Institution Contribution Number 11292.

Corresponding author address: Dr. Steven J. Lentz, Physical Oceanography, Woods Hole Oceanographic Institution, MS #21, Woods Hole, MA 02543.
E-mail: slentz@whoi.edu

layer (e.g., Trowbridge and Lentz 1991; MacCready and Rhines 1993; Garrett et al. 1993). Furthermore, the reduction in bottom stress alters the adjustment of the overlying flow such that narrow alongshelf currents can, in principle, persist for long distances and times (e.g., Chapman and Lentz 1997; Chapman 2002).

The previous theoretical studies mentioned above each examined the impact of buoyancy advection in the bottom boundary layer by postulating the existence of an alongshelf current in the presence of initially horizontal isopycnals. The current then generates a bottom boundary layer in which buoyancy is advected up or down the slope. These studies provide valuable insight into the effects of buoyancy advection, but the initial condition is a bit contrived. That is, the origin of the initial alongshelf current is not considered, and there is no explanation for how the current appears while the isopycnals remain undisturbed. Thus, these studies cannot elucidate the dynamics of the acceleration process, nor can they provide estimates of the forced currents that could be achieved in the presence of buoyancy advection in the bottom boundary layer. Here we consider a two-dimensional flow starting from rest, accelerated by a prescribed alongshelf pressure gradient. Previous studies of the wind-driven upwelling response of a stratified ocean found a steady state was reached over a diffusive time scale associated with the horizontal eddy viscosity (Allen 1973; Hamilton and Rattray 1978). Horizontal diffusion is neglected here to focus on the acceleration of a stratified current and because of the uncertainty in the magnitude of the horizontal eddy viscosity and the processes contributing to horizontal diffusion. An idealized theoretical model for the response to either an upwelling or a downwelling pressure gradient is developed in section 2, with the results following in section 3. Numerical model calculations are used in section 4 to support the theoretical model results. Applications to wind forcing are considered in section 5. The results are discussed and summarized in section 6.

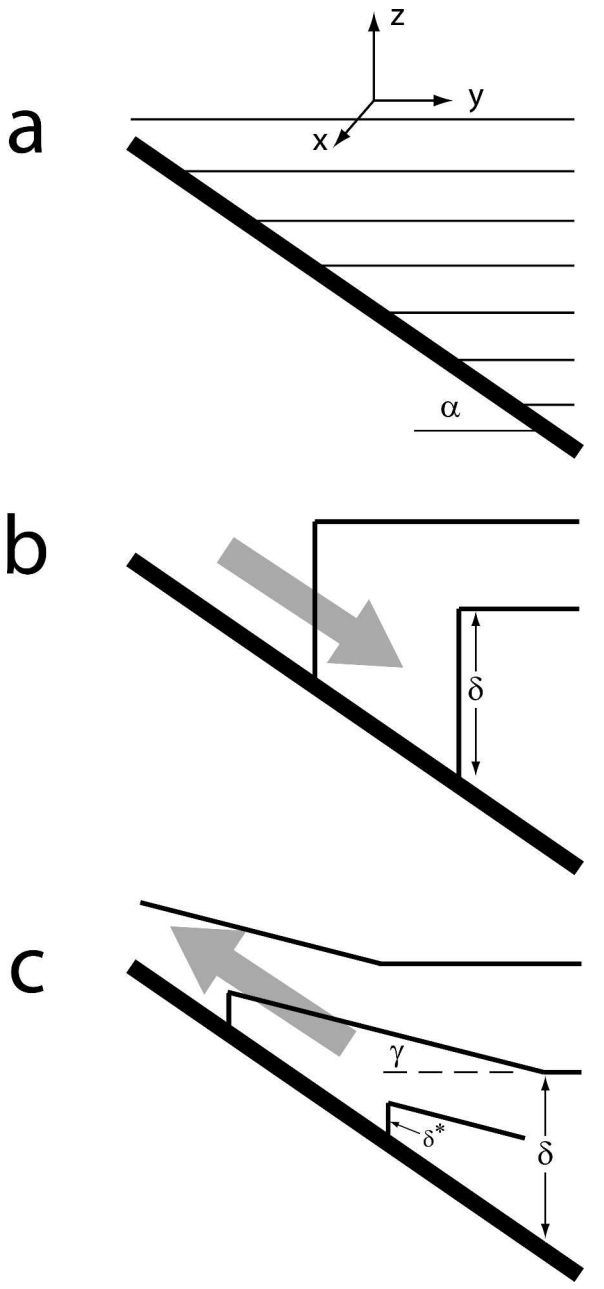

FIG. 1. Schematic of (a) the initial resting state of a stratified fluid over a uniformly sloping bottom, (b) the density structure of a downwelling bottom boundary layer, and (c) the density structure of an upwelling bottom boundary layer. Gray arrows indicate direction of flow in the boundary layer. Bottom slope is α, and total boundary layer thickness is δ. For upwelling, isopycnal angle is γ and mixed layer thickness is δ^*.

2. Theory

The model formulation is similar to that of Chapman (2002). The flow is assumed hydrostatic and two-dimensional (Fig. 1) with no variations along the isobaths (x direction). The alongshelf velocity, u, is assumed to be in geostrophic balance throughout the water column and at all times, except for a bottom mixed layer in the upwelling case (described in section 2b). Advection of momentum is assumed negligible, but advection of density is included. An alongshelf pressure gradient, P_x, is prescribed as a forcing function in the alongshelf momentum equation. With these assumptions, the equations of motion are

$$u_t - fv = -P_x/\rho_0 + \tau^x_z/\rho_0, \quad (1)$$

$$fu = -p_y/\rho_0, \quad (2)$$

$$0 = p_z + g\rho, \quad (3)$$

$$v_y + w_z = 0, \quad \text{and} \quad (4)$$

$$\rho_t + v\rho_y + w\rho_z = D_z, \quad (5)$$

where (u, v, w) are the velocity components in the alongshelf (x), cross-shelf (y), and vertical (z) directions, respectively; p is pressure; ρ is the density anomaly relative to the constant surface density ρ_0; f is the Coriolis parameter; τ^x is the stress in the x direction; D is the vertical turbulent density flux; and g is gravitational acceleration. Subscripts y, z, and t denote partial differentiation. For convenience, the density anomaly ρ is referred to as the density.

The surface ($z = 0$) is assumed rigid, so (4) may be integrated vertically from the bottom at $z = -h(y)$ to the surface to obtain

$$\frac{\partial}{\partial y}\left(\int_{-h}^{0} v\, dz\right) = 0.$$

Since $v = 0$ at the coast, then $\int_{-h}^{0} v\, dz = 0$ everywhere. This means that the flow away from the influence of the coast, while physically two-dimensional, is mathematically locally one-dimensional because y only enters parametrically through the depth h.

Vertical integration of (1) produces

$$\frac{\partial}{\partial t}\int_{-h}^{0} u\, dz = -hP_x/\rho_0 - ru^b, \quad (6)$$

where P_x has been assumed independent of depth, there is no surface stress, and a linear bottom stress law has been applied, namely, $\tau^x = \rho_0 ru$ at $z = -h$ with r being a constant friction coefficient and u^b the velocity evaluated at the bottom.

The flow is initially at rest with horizontal isopycnals (Fig. 1a). The initial density field is given by

$$\rho = -\rho_0 N^2 z/g, \quad (7)$$

where N is a constant buoyancy frequency. As the pressure gradient is applied, the water accelerates in the x direction, rapidly forming a bottom Ekman layer with cross-shelf transport. Buoyancy is advected downslope (upslope) for a negative (positive) pressure gradient. In the downwelling case (Fig. 1b), lighter water is carried under heavier water, creating an unstable density field that mixes rapidly to form a thick boundary layer. In the upwelling case (Fig. 1c), denser water is carried upslope, producing a thin boundary layer. This difference was first discussed by Weatherly and Martin (1978) and has since been studied extensively (see Garrett et al. 1993). In both cases, according to (6), a steady state may be reached if the bottom stress becomes large enough to balance the imposed pressure gradient, that is, if $u^b = -hP_x/\rho_0 r$. However, the time required to reach steady state may be long, and there is no guarantee that a steady state is ever achieved.

Regardless of the sign of the forcing, buoyancy advection generates horizontal density gradients in the bottom boundary layer, which produce vertical shear in the alongshelf velocity according to the thermal-wind balance, found by combining (2) and (3) to form

$$u_z = g\rho_y/\rho_0 f. \quad (8)$$

Given an expression for ρ_y in the bottom boundary layer, the thermal wind balance (8) can be used with (6) to obtain an equation for u. To proceed, we consider downwelling and upwelling separately because of the differences in the bottom boundary layer structure for the two cases (see Fig. 1).

a. Downwelling

In a downwelling bottom boundary layer, the density is vertically well mixed (Fig. 1b), so ρ_y is independent of z and (8) can be integrated from the top of the bottom boundary layer to a depth z within the boundary layer to obtain

$$u = u^i - \frac{g}{\rho_0 f}\rho_y(\delta - h - z) \quad -h \le z \le -h + \delta, \quad (9)$$

where δ is the thickness of the bottom boundary layer and u^i is the interior velocity above the bottom boundary layer. From (7) and considering a uniformly sloping bottom,

$$\rho_y = \rho_0 \alpha N^2/g \quad -h \le z \le -h + \delta, \quad (10)$$

where α is the bottom slope and we assume $\alpha \ll 1$. Substituting (10) into (9) produces

$$u = u^i - \frac{\alpha N^2}{f}(\delta - h - z) \quad -h \le z \le -h + \delta, \quad (11)$$

which may be substituted into (6) to obtain

$$\frac{du^i}{dt} + \frac{r}{h}u^i = \frac{\alpha N^2}{fh}\left(\frac{1}{2}\frac{d\delta^2}{dt} + r\delta\right) - \frac{1}{\rho_0}P_x. \quad (12)$$

An expression for δ is found by integrating (5) from the bottom to the top of the bottom boundary layer (remembering that $\rho_z = 0$ in the bottom boundary layer and $D = 0$ at both $z = -h$ and $z = -h + \delta$). Then, (1)

is used to define v within the boundary layer, assuming no stress at the top of the boundary layer, to obtain

$$\delta\rho_t + \rho_y\left(\frac{\delta}{f}\frac{du^i}{dt} - \frac{\alpha N^2}{f^2}\frac{1}{2}\frac{d\delta^2}{dt} + \frac{1}{\rho_0 f}P_x\delta + \frac{r}{f}u^b\right) = 0. \tag{13}$$

From (7) evaluated at $z = -h + \delta$, we can write $\rho_t = -\rho_0 N^2\delta_t/g$. Substituting this result, along with (10) and (11), into (13) yields

$$\frac{1}{2}\frac{d\delta^2}{dt}\left(1 + \frac{\alpha^2N^2}{f^2}\right) = \frac{\alpha\delta}{f}\frac{du^i}{dt} + \frac{\alpha}{\rho_0 f}P_x\delta + \frac{\alpha r}{f}\left(u^i - \frac{\alpha N^2}{f}\delta\right). \tag{14}$$

Equations (12) and (14) define the growth of the interior velocity and the bottom boundary layer in response to an imposed downwelling pressure gradient. These equations can be simplified by an appropriate scaling of variables. For example, if t is scaled by the friction time scale h/r, δ by depth h, u^i by fh/α, and P_x by $\rho_0 fr/\alpha$, then (12) and (14) may be written as

$$\frac{du^i}{dt} + u^i = S^2\left(\frac{1}{2}\frac{d\delta^2}{dt} + \delta\right) - P_x \quad \text{and} \tag{15}$$

$$\frac{1}{2}\frac{d\delta^2}{dt} = \frac{1}{1+S^2}\left(\delta\frac{du^i}{dt} + P_x\delta + u^i - S^2\delta\right), \tag{16}$$

where $S = N\alpha/f$ is the Burger number, and all variables are now in scaled form. The problem is now completely defined by the prescribed pressure gradient forcing P_x and the Burger number S.

b. Upwelling

An upwelling bottom boundary layer has a more complicated structure than the downwelling boundary layer (Fig. 1c). Based on the work of Weatherly and Martin (1978) and Trowbridge and Lentz (1991), we assume that the boundary layer consists of two parts: a mixed layer at the bottom and a geostrophic shear layer above. The mixed layer grows rapidly after the onset of forcing, essentially like that over a flat bottom, with thickness $\delta^* = u_*/(Nf)^{1/2}$, where u_* is the shear velocity defined by $u_* = (\tau^x/\rho_0)^{1/2}$ at $z = -h$. We further assume that δ^* is constant in time and that there is no vertical shear in this layer. That is, the combined effects of lateral density gradients and frictional shear maintain a vertically uniform velocity within this layer. The bottom stress that forms this layer is approximated by $\tau^x \approx -hP_x$, so

$$\delta^* \approx \left(\frac{h}{\rho_0 Nf}P_x\right)^{1/2}. \tag{17}$$

The cross-shelf flow associated with Ekman transport in the bottom boundary layer carries the isopycnals up the slope, forming a region of sloping isopycnals above the mixed layer that we call the geostrophic shear layer. The total boundary layer thickness is δ. We assume that the isopycnals in the geostrophic shear layer ($\delta - \delta^*$) remain linear, forming an angle γ with the horizontal (we assume $\gamma \ll 1$), while the interior isopycnals ($z > -h + \delta$) remain horizontal (Fig. 1c). We will show in section 4 that these assumptions are basically consistent with numerical model calculations that include full two-dimensional dynamics. Given this density structure, the velocity in the geostrophic shear layer is found by integrating (8) to obtain

$$u = u^i - \frac{g}{\rho_0 f}\rho_y(\delta - h - z) \quad -h + \delta^* \le z \le -h + \delta. \tag{18}$$

The cross-shelf density gradient in the geostrophic shear layer can be written as

$$\rho_y = -\frac{\rho_0 N^2}{g}\left(\frac{\alpha\gamma}{\alpha - \gamma}\right), \tag{19}$$

which, when substituted into (18), yields

$$u = u^i + \frac{\alpha N^2}{f}\Gamma(\delta - h - z) \quad -h + \delta^* \le z \le -h + \delta, \tag{20}$$

where $\Gamma = \gamma/(\alpha - \gamma)$. The alongshelf velocity in the mixed layer is given by the velocity at the bottom of the geostrophic shear layer,

$$u = u^b = u^i + \frac{\alpha N^2}{f}\Gamma(\delta - \delta^*) \quad -h \le z \le -h + \delta^*. \tag{21}$$

The horizontal density gradient in the geostrophic shear layer and, hence, the thermal-wind shear, increase with γ, becoming infinite when the isopycnals are parallel to the bottom; that is, $\Gamma \to \infty$ as $\gamma \to \alpha$. This is clearly not a physical possibility. In fact, we expect the isopycnal slope in the geostrophic shear layer to be limited by shear instability that produces mixing. That is, there should be a balance between the tendency for upwelling to increase the shear while mixing reduces the shear. To quantify, we assume that the isopycnal slope reaches a constant value determined by a critical gradient Richardson number in the geostrophic shear layer. The Richardson number is here defined as Ri =

$N^2_{gsl}/(u_z)^2$, where $N^2_{gsl}=N^2\alpha/(\alpha-\gamma)$ is the squared buoyancy frequency in the geostrophic shear layer, from the geometry

$$\rho_z = -\frac{\rho_0 N^2}{g}\left(\frac{\alpha}{\alpha-\gamma}\right),$$

and u_z is the thermal-wind shear. From (8), $\mathrm{Ri} = (1+\Gamma)/S^2\Gamma^2$, which can be rearranged to provide an estimate for Γ as

$$\Gamma = \frac{1+(1+4S^2\mathrm{Ri}_c)^{1/2}}{2S^2\mathrm{Ri}_c}, \tag{22}$$

where Ri_c is the critical Richardson number, chosen here to be unity. Given a constant value of Γ from (22), substitution of (20) and (21) into (6) then produces

$$\frac{du^i}{dt}+\frac{r}{h}u^i = -\frac{\alpha N^2}{fh}\Gamma\left[(\Delta+\delta^*)\frac{d\Delta}{dt}+r\Delta\right]-\frac{1}{\rho_0}P_x, \tag{23}$$

where $\Delta = \delta - \delta^*$ is the thickness of the geostrophic shear layer.

After the initial formation of the mixed layer and the establishment of the isopycnal slope in the geostrophic shear layer, we assume that the upslope movement of isopycnals is purely advective. Further, we assume that the cross-shelf velocity is uniform in the mixed layer and decreases linearly to zero at $z = -h+\delta$. Thus, $v = v^b$ in the mixed layer and $v = v^b\,(\delta - h - z)/(\delta-\delta^*)$ in the geostrophic shear layer, where v^b is the cross-shelf velocity at the bottom. Using this expression for v along with (20) and (21), we can integrate (1) through the bottom boundary layer to obtain

$$v^b\left(\frac{\delta+\delta^*}{2}\right) = \frac{1}{f}\frac{du^i}{dt}\delta+\frac{\alpha N^2}{f^2}\Gamma\frac{d\Delta}{dt}(\Delta+\delta^*)+\frac{1}{\rho_0 f}P_x\delta + \frac{r}{f}\left(u^i+\frac{\alpha N^2}{f}\Gamma\Delta\right). \tag{24}$$

By definition, $v^b = -dy^b/dt$ where y^b is the distance each isopycnal has moved along the bottom. This definition can be used with (24) and simple geometry to obtain

$$\frac{d\Delta}{dt}\left[\frac{\delta+\delta^*}{2}+S^2(\Delta+\delta^*)\right] = -\frac{\alpha}{\Gamma}\left[\frac{1}{f}\frac{du^i}{dt}\delta+\frac{1}{\rho_0 f}P_x\delta + \frac{r}{f}\left(u^i+\frac{\alpha N^2}{f}\Gamma\Delta\right)\right]. \tag{25}$$

Equations (23) and (25) define the growth of the interior velocity and the geostrophic shear layer in response to an imposed upwelling pressure gradient. As in the downwelling case, they can be simplified by scaling t by h/r, u^i by fh/α and δ by h to produce

$$\frac{du^i}{dt}+u^i = -S^2\Gamma\left[(\Delta+\delta^*)\frac{d\Delta}{dt}+\Delta\right]-P_x \tag{26}$$

and

$$\frac{d\Delta}{dt} = -\frac{1}{\Gamma}\left[\frac{\delta+\delta^*}{2}+S^2(\Delta+\delta^*)\right]^{-1} \times\left(\delta\frac{du^i}{dt}+P_x\delta+u^i+S^2\Gamma\Delta\right), \tag{27}$$

where all variables are now in scaled form. Note that the form of (26) and (27) is quite similar to that of the downwelling case, (15) and (16). In fact, if $\Gamma = 1$ and $\delta^* = 0$ (making $\Delta = \delta$) and keeping in mind that u and P_x have opposite signs, then the forms are identical except for the factor of 1/2 in the first set of square brackets in (27), which results from the assumed vertical structure of v in the upwelling case.

After scaling, the mixed layer thickness (17) becomes

$$\delta^* = \left[\left(\frac{r}{fh}\right)\frac{1}{S}P_x\right]^{1/2}. \tag{28}$$

This introduces another parameter, r/fh, which is the ratio of the inertial time scale f^{-1} to the friction time scale h/r, and is typically small except in very shallow water. Using (22) and (28) with (26) and (27), the problem at each depth is now defined by the prescribed pressure gradient forcing P_x, the Burger number S, and r/fh.

3. Theoretical results

a. Downwelling

The downwelling pressure gradient is negative, so the interior flow accelerates in the $+x$ direction, according to (15). The u^i term in (15) represents friction acting on the interior flow, as if u^i extended to the bottom. However, frictional effects are limited by the reduction in bottom velocity due to thermal-wind shear in the bottom boundary layer ($S^2\delta$) and the tendency for the boundary layer to grow (first term in the brackets). From (16), boundary layer growth is driven by the cross-shelf transport in the bottom boundary layer; bottom stress produces downslope transport proportional to $u^b = u^i - S^2\delta$, augmented by a small contribution from the interior acceleration ($\delta du^i/dt$), while the pressure gradient contributes an upslope geostrophic transport ($P_x\delta < 0$).

With no stratification ($S = 0$), the solution to (15) for constant P_x is

$$u^i = -P_x(1 - e^{-t}). \tag{29}$$

The interior velocity (which is depth-independent in this case, so $u^b = u^i$) increases until reaching a steady state in which it balances the imposed pressure gradient. The dimensional e-folding time scale is h/r. This is the standard behavior when buoyancy advection in the bottom boundary layer is not possible.

With stratification, the growth of the boundary layer reduces the bottom velocity relative to the interior velocity; that is, $u^b = u^i - S^2\delta$. This reduces bottom stress and allows both the boundary layer thickness and interior velocity to continue to increase for many friction time scales. According to (15) and (16), a steady state is eventually reached when $\delta = 1$ and $u^i = S^2 - P_x$; that is, the boundary layer has grown to the depth of the water column, leaving vertical isopycnals everywhere. However, this steady state is not physically achievable because all of the interior fluid must be mixed into the bottom boundary layer. Furthermore, the time required to reach steady state is so long for all but the smallest S that it is unlikely such a steady state exists in the ocean.

To demonstrate, we have computed solutions of (15) and (16) numerically using standard ordinary-differential-equation solvers available in MATLAB. A reasonable value for P_x is obtained as follows. A sea surface slope of -10^{-7} is consistent with previous models (e.g., Zamudio and Lopez 1994) and observations (e.g., Scott and Csanady 1976; Hickey 1984). In the absence of bottom friction, this sea surface slope would accelerate the entire water column by about 0.1 m s^{-1} in one day,[1] being equivalent to unscaled $P_x/\rho_0 = -10^{-6}$ m s^{-2}. Taking $f = 10^{-4}$ s^{-1}, $r = 5 \times 10^{-4}$ m s^{-1}, and $\alpha = 0.001$ to 0.005, then $(\alpha/\rho_0\, fr)P_x$ is in the range -0.02 to -0.1. Figure 2 shows solutions of (15) and (16) for $P_x = -0.02$ and a range of Burger numbers. For comparison, the dotted line in Fig. 2a is the interior velocity with no bottom friction, while the dotted curve in Fig. 2b is the bottom velocity with no stratification. For each Burger number, the interior velocity, bottom velocity and boundary layer thickness each increase with time. Only the weakest stratification ($S = 0.2$) reaches a steady state after 20 friction time scales, while in all other cases, the interior velocity continues to accelerate. Stronger stratification produces faster acceleration while maintaining a smaller bottom velocity and a thinner bottom boundary layer, that is, smaller bottom stress. For $S = 1.5$, the interior velocity accelerates almost as fast as the frictionless case; that is, bottom stress is nearly zero.

[1] Found by solving (12) with $r = 0$ and $N = 0$, after replacing P_x/ρ_0 with $g\zeta_x$, where ζ is the sea-surface elevation.

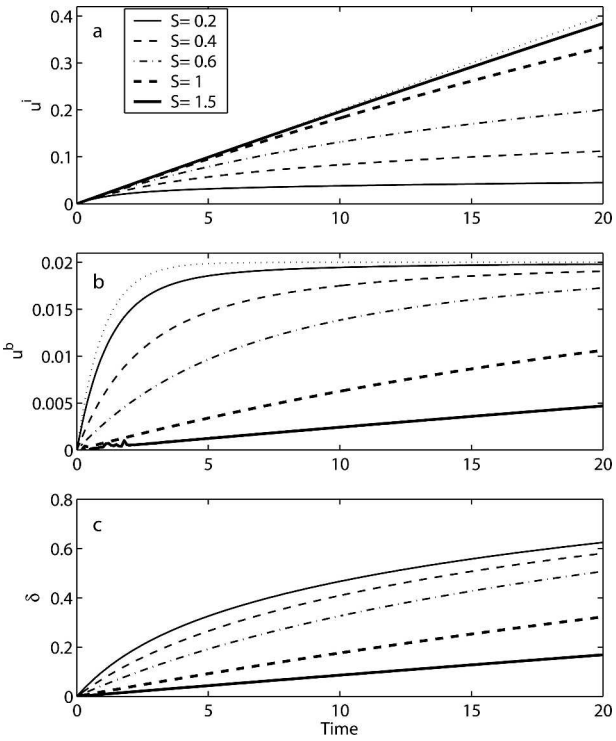

FIG. 2. Response to a downwelling pressure gradient ($P_x = -0.02$) for various values of Burger number S: (a) interior velocity, (b) bottom velocity, and (c) bottom boundary layer thickness. All variables have been scaled as stated in text. Dotted line in (a) is the response with no bottom friction. Dotted curve in (b) is the response with no stratification ($S = 0$).

Figure 3 compares the interior velocity obtained after 10 friction time scales to the steady-state interior velocity obtained in the unstratified case, for a range of Burger numbers and pressure gradients. Stratification clearly produces a substantial increase in interior velocity, even for fairly small Burger numbers. Note that the stratified flow is still accelerating after 10 friction time scales, so the ratios shown in Fig. 3 will continue to increase with time. The point is that even relatively weak stratification can have a major impact on currents generated by pressure gradient forcing, producing large interior velocities with little bottom stress.

b. *Upwelling*

The upwelling pressure gradient is positive, so the interior flow accelerates in the $-x$ direction, according to (26). Much like the downwelling case, frictional effects on the interior flow (u^i term) are limited by the reduction in bottom velocity due to thermal-wind shear in the geostrophic shear layer ($-S^2\Gamma\Delta$) and the tendency for the geostrophic shear layer to grow (first term in the square brackets). From (27), geostrophic shear

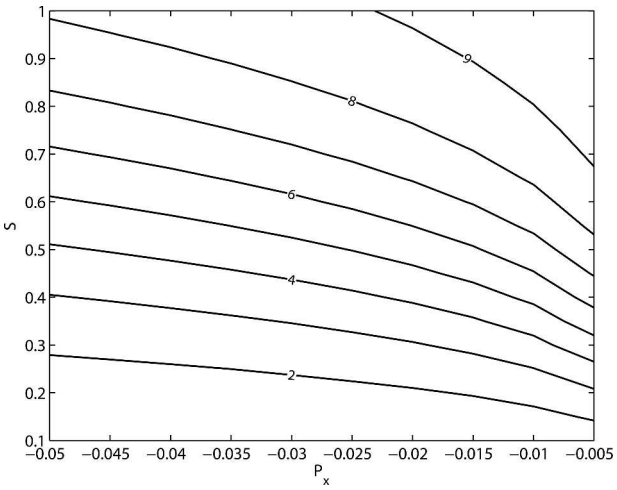

FIG. 3. Interior alongshelf velocity u^i from the theoretical model after 10 friction time scales, relative to the unstratified steady-state velocity, contoured over a range of downwelling pressure gradients and Burger numbers.

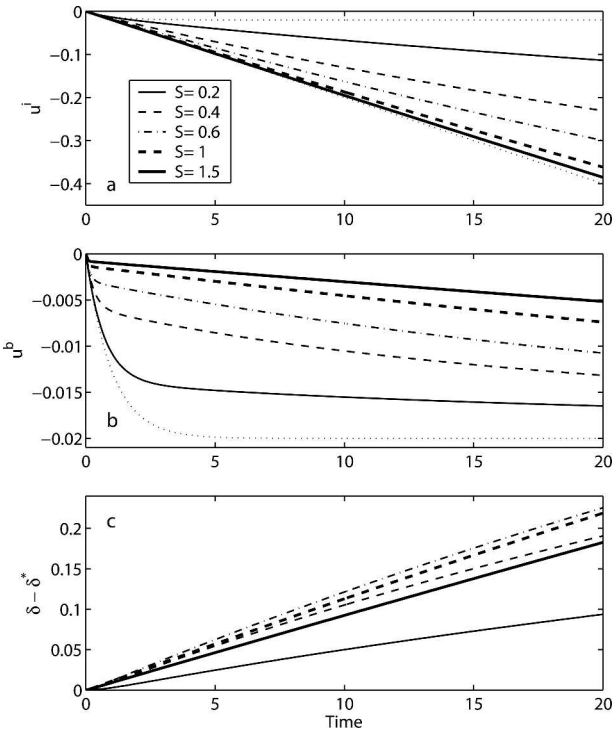

FIG. 4. Response to an upwelling pressure gradient ($P_x = 0.02$, $r/fh = 0.0625$) for various values of Burger number S: (a) interior velocity, (b) bottom velocity, and (c) geostrophic shear layer thickness. All variables have been scaled as stated in text. The $S = 1.5$ curve in (a) overlies the response with no bottom friction. Dotted curves in (a) and (b) are the response with no stratification ($S = 0$).

layer growth is driven by the upslope transport caused by bottom stress, proportional to $u^b = u^i + S^2\Gamma\Delta$ and augmented by the interior acceleration, while the pressure gradient contributes a downslope geostrophic transport ($P_x\delta > 0$).

The limit of no stratification ($S = 0$) is peculiar because of our choice of Γ, given by (22). To maintain a critical Richardson number of 1, both the buoyancy frequency and the vertical shear in the geostrophic shear layer must become infinite as $S \to 0$, clearly an unreasonable requirement. This suggests that (22) probably does not hold for small S. The unstratified case is recovered by holding Γ constant and letting S vanish in (26), for which the solution is then again given by (29). The unstratified response is identical to the downwelling case, except that the flow direction is reversed.

With stratification, the growth of the geostrophic shear layer reduces the velocity at the bottom, $u^b = u^i + S^2\Gamma\Delta$, which allows the interior velocity to continue to accelerate well beyond the unstratified steady-state limit. There is again a theoretical steady state in which $\delta = 1$ and $u^i = -S^2\Gamma\ (1 - \delta^*)$; however, it is unclear how the steady state could be achieved given the assumed structure of the boundary layer.

Figure 4 shows the temporal evolution of u^i, u^b, and Δ for a variety of Burger numbers, obtained numerically using standard ordinary-differential-equation solvers in MATLAB. The dotted curves in Figs. 4a and 4b represent the response with no stratification. The $S = 1.5$ curve in Fig. 4a overlies the frictionless response. As expected, the geostrophic shear layer continues to grow, keeping u^b small and allowing u^i to continue to accelerate for many friction time scales. Even for the weakest stratification ($S = 0.2$), the interior velocity is still increasing after 20 friction time scales.

Figure 5 shows the interior velocity after 10 friction time scales compared to the unstratified steady-state velocity, for a range of Burger numbers and pressure gradients. The increase over the unstratified case is even more dramatic than for the downwelling case in Fig. 3. And, the interior current continues to increase long after 10 friction time scales. As in the downwelling case, stratification has a major effect on currents generated by pressure gradient forcing, producing large interior velocities with little bottom stress.

4. Comparison with a numerical model

Many of the assumptions made in developing the above theoretical models are not easily justifiable a priori, so it is useful to compare the theory with two-dimensional numerical model calculations in which the dynamics are more complete. Our intention is not a

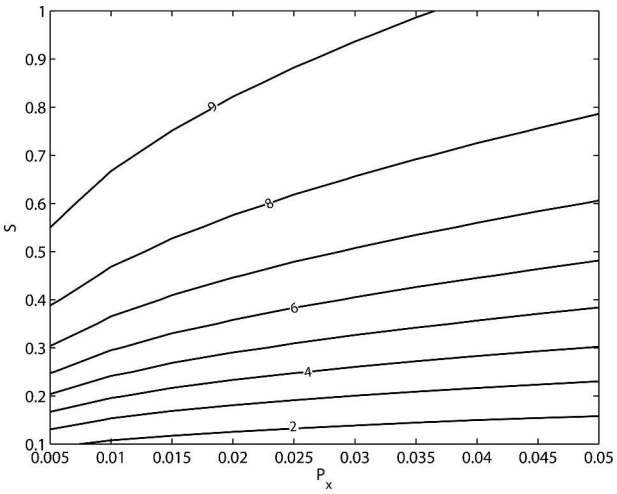

FIG. 5. Interior alongshelf velocity u^i from the theoretical model after 10 friction time scales, relative to the unstratified steady-state velocity, contoured over a range of upwelling pressure gradients and Burger numbers ($r/fh = 0.0625$).

detailed analysis of the numerical model results. This has been done previously for similar problems (e.g., Chapman 2000, 2002), and the theory will no doubt suffer from similar deficiencies (e.g., the neglect of cross-shelf stresses and the lack of changes in the interior density field). Instead, the goal here is to establish some degree of credibility for the theoretical model by showing that the assumptions and results are qualitatively and, to a large extent, quantitatively reasonable.

We use the Regional Ocean Model System (ROMS) in a two-dimensional configuration. ROMS is a free-surface, hydrostatic, primitive equation ocean model that uses stretched, terrain-following coordinates in the vertical and orthogonal curvilinear coordinates in the horizontal. Details can be found on the ROMS Web site (available online at http://marine.rutgers.edu/po/index.php?model=roms). The model is here configured in two dimensions (cross-shelf and vertical), in a periodic channel with length 2 km, using four alongshelf grid points with no alongshelf variations. The topography is given by $h = h_0 + \alpha y$, where $h_0 = 10$ m is the depth at the coast and $\alpha = 0.001$. An offshore wall is located 200 km from the coast and does not impact the results presented here. Horizontal grid spacing is 1 km, while 30 vertical grid points are used with grid points concentrated near the bottom to resolve the bottom boundary layer. Standard dynamical assumptions are made: no flow or density flux through solid boundaries, linearized bottom stress with a coefficient of $r = 5 \times 10^{-4}$ m s^{-1}, Mellor–Yamada level-2.5 turbulence closure scheme, uniform rotation with $f = 10^{-4}$ s^{-1}, and no explicit lateral mixing or viscosity. The ocean is initially at rest with a constant buoyancy frequency N. A constant, spatially uniform alongshelf pressure gradient is applied as a body force over the entire domain. The baroclinic time step is between 72 and 288 s, depending on the stratification, while the barotropic time step is 1/30 of the baroclinic time step.

Obviously, the theory will not apply close to the coast or the offshore wall, where the bottom boundary layer is interrupted and vertical velocities may be substantial. However, the vigor of the cross-shelf circulation is determined by the bottom Ekman transport, which is proportional to the bottom stress. For most stratified flows, the cross-shelf circulation is quite weak, so the region of coastal influence remains small for a very long time. Therefore, comparisons are made here at locations away from the coast, but in the shallower parts of the domain where the vertical resolution is better, say 40–90 km away from the coast.

Figure 6 compares the numerical and theoretical responses to a downwelling pressure gradient for three choices of Burger number, at $y = 70$ km offshore. The surface velocity is used to represent the interior velocity in the numerical results. Other locations produce nearly identical comparisons. The theoretical and numerical models agree fairly well, although the numerical model velocities are smaller than the theoretical velocities as S increases. Also, the numerical bottom velocity becomes highly variable at long times ($t > 7$) for larger S. This is caused by instabilities in the bottom boundary layer (Allen and Newberger 1998), which are not possible in the theory. However, they do not appear to impact the interior acceleration.

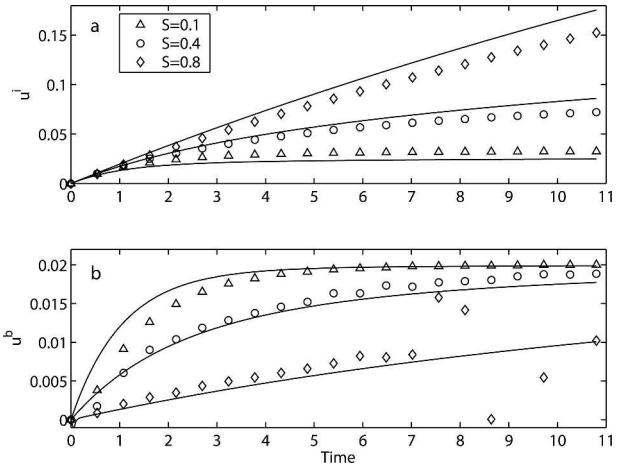

FIG. 6. Comparison of the theoretical (solid curves) and numerical model (symbols) time responses to a downwelling pressure gradient of $P_x = -0.02$ and for several Burger numbers ($S = 0.1$, 0.4, 0.8): (a) interior and (b) bottom velocities at $y = 70$ km offshore. All variables are scaled as stated in text.

Figure 7 compares the vertical structure of the alongshelf velocity at $t = 8$ and $y = 70$ km offshore for three Burger numbers. Again the numerical velocities are slightly weaker than the theoretical velocities for larger S, but the vertical structure is strikingly similar; the bottom boundary layer thickness, the vertical shear in the bottom boundary layer and the nearly vertically uniform interior velocity all match the theory quite well. For very weak stratification ($S = 0.1$), the numerical model resolves the bottom Ekman layer, which is absent in the theory, and produces a different vertical structure with stronger currents.

An upwelling pressure gradient rapidly produces a bottom boundary layer in the numerical model with structure much like that sketched in Fig. 1c. In particular, a mixed layer forms at the bottom with a geostrophic shear layer of tilted isopycnals above. The isopycnals in the geostrophic shear layer quickly reach a nearly constant slope and the entire structure moves up the sloping bottom. Figure 8 shows the time evolution of a single isopycnal (originally at 50-m depth) for three different Burger numbers. The mixed layer is evident in each case, being much thinner for larger S, as in (28). The slope of the isopycnal is nearly constant after an initial adjustment period. These features are clearly consistent with the assumed structure of the theoretical model.

It is interesting to note that the isopycnal in the intermediate case ($S = 0.4$) moves upslope faster than either the weaker or stronger stratification cases. The explanation may be found in the cross-shelf bottom velocity (24). Weak stratification produces a larger mixed layer δ^*, according to (28). This reduces v^b, according to (24), by spreading the cross-shelf flow over a thicker boundary layer, so the isopycnals for weak stratification move upslope slowly. Strong stratification produces a thinner mixed layer, but also large vertical shear in the geostrophic shear layer, $(\alpha N^2/f)\Gamma\Delta$ in (24). This reduces v^b, hence slowing the upslope movement of the isopycnals. The fastest upslope movement occurs at intermediate stratification, where neither the mixed layer nor the geostrophic shear layer is too large. Unfortunately, the theoretical model does not capture this interesting behavior because of quantitative differences between (28) and the mixed layer thickness produced by the numerical model.

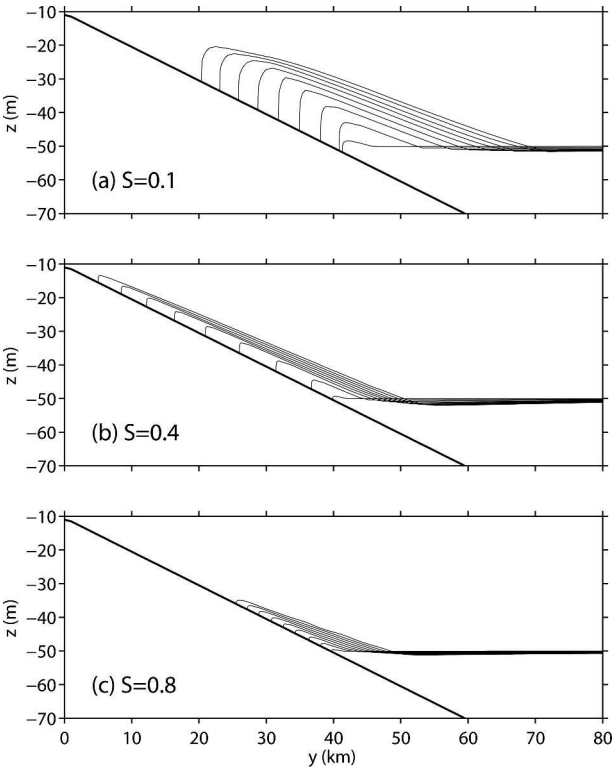

FIG. 8. Time evolution of a single isopycnal (originally at 50-m depth) from the numerical model for three different Burger numbers. Isopycnals are plotted every 2 days.

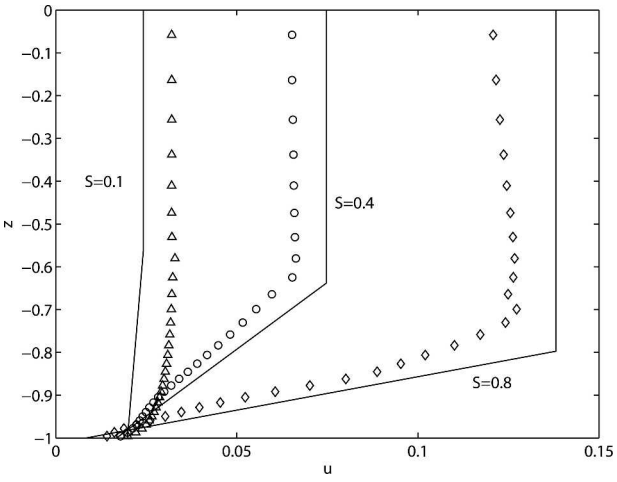

FIG. 7. Comparison of the theoretical (solid curves) and numerical model (symbols) velocity profiles at $t = 8$ and $y = 70$ km offshore in response to a downwelling pressure gradient of $P_x = -0.02$ and for several Burger numbers. All variables are scaled as stated in text.

We have assumed in (22) that the slope of the isopycnals in the geostrophic shear layer is such that the local gradient Richardson number is 1. To test this in the numerical model calculations, we have computed the local gradient Richardson number everywhere in the model domain and plotted the values against the local buoyancy frequency N (Fig. 9). The largest N occurs within the geostrophic shear layer. Above the geostrophic shear layer, $\mathrm{Ri} \to \infty$ because N remains close to the initial buoyancy frequency and $u_z \approx 0$. In the mixed

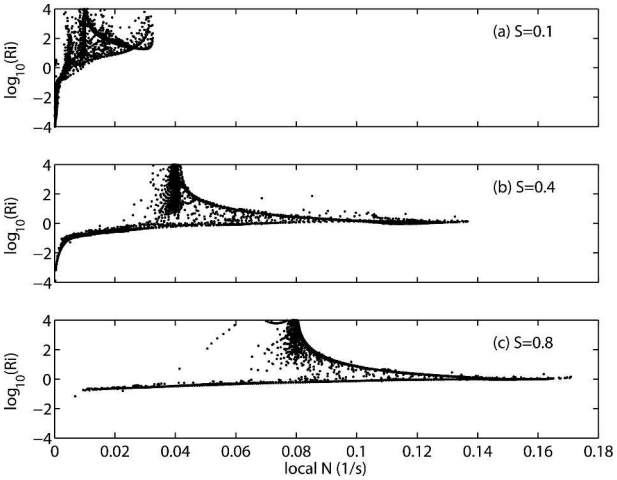

FIG. 9. Local gradient Richardson number at each grid point in the numerical model plotted against the local buoyancy frequency, for three different Burger numbers. The largest N occurs in the geostrophic shear layer, where Ri ≈ 1 for $S = 0.4$ and 0.8.

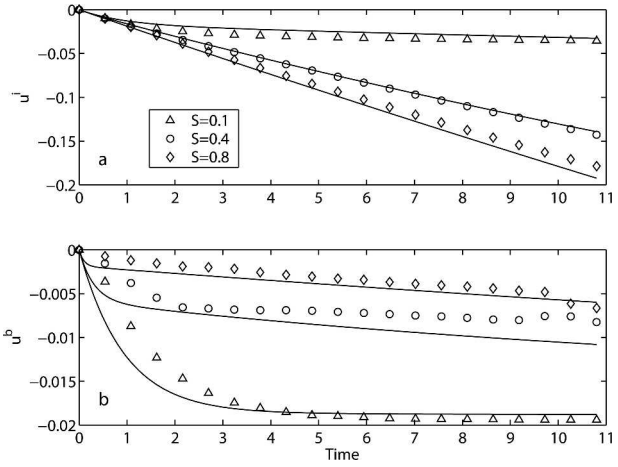

FIG. 10. Comparison of the theoretical (solid curves) and numerical model (symbols) time responses to an upwelling pressure gradient of $P_x = 0.02$ and for several Burger numbers ($S = 0.1$, 0.4, 0.8): (a) interior and (b) bottom velocities at $y = 70$ km offshore. All variables are scaled as stated in text.

layer Ri ≈ 0 because $N \approx 0$. For $S = 0.4$ and 0.8, Ri is close to unity for the largest N, that is, in the geostrophic shear layer, consistent with our assumption. (Individual profiles also show this result.) For weak stratification ($S = 0.1$), Ri in the geostrophic shear layer is considerably larger than unity, suggesting that the response is basically frictional and is not dominated by buoyancy advection, unlike the other two cases. This is also consistent with our argument in section 3b that the gradient Richardson number cannot remain at one as $S \to 0$.

Figure 10 compares the responses of the theoretical and numerical models with an upwelling pressure gradient for three Burger numbers. The comparison is fairly good except for the bottom velocity at early times. Clearly, the tendency for the bottom velocity to remain small while the interior velocity continues to increase is present in the numerical results. Similarly, Fig. 11 shows that the vertical structure of the alongshelf velocity is similar for both the theoretical and numerical models, indicating that the basic assumptions of the theory are reasonable. For weak stratification, the numerical model again develops more of an Ekman layer rather than a geostrophic shear layer, which alters the vertical structure considerably.

5. Application to wind forcing

It is straightforward to use the present approach to investigate some aspects of wind-driven downwelling and upwelling. A uniform wind stress applied to a two-dimensional model generally produces three regions with different responses: (i) a well-mixed region close to the coast, (ii) a region of geostrophic shear with a strong surface-intensified alongshelf current, and (iii) a region farther offshore in which the interior isopycnals are essentially undisturbed (e.g., Austin and Lentz 2002; Lentz and Chapman 2004). The interior velocity in region (iii) is nearly vertically uniform, as assumed for the pressure gradient forcing described above, so (1) can be integrated to obtain

$$\frac{\partial}{\partial t}\int_{-h}^{0} u\, dz = \frac{\tau^s}{\rho_0} - ru^b \tag{30}$$

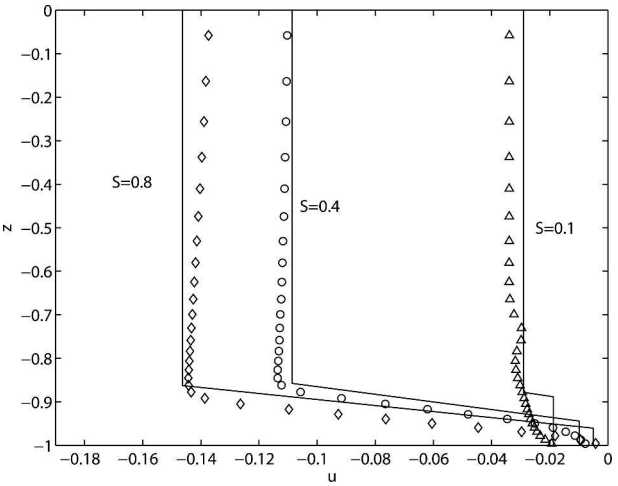

FIG. 11. Comparison of the theoretical (solid curves) and numerical model (symbols) velocity profiles at $t = 8$ and $y = 70$ km offshore in response to an upwelling pressure gradient of $P_x = 0.02$ and for several Burger numbers. All variables are scaled as stated in text.

instead of (6), where τ^s is the applied alongshelf surface wind stress. The derivation of (15) for a downwelling wind and (26) for an upwelling wind proceeds as above, but with the scaled pressure gradient replaced by the scaled wind stress, $(\alpha/\rho_0 fr)\tau^s/h$. Likewise, the definition of the mixed layer thickness (28), for wind-driven upwelling, requires that P_x be replaced by the scaled wind stress. The derivation of (16) and (27) is unchanged, except that $P_x = 0$ in the wind-forced case. The wind stress does not appear in the equivalent of (16) and (27) because it does not extend through the water column, as does the pressure gradient.

Clearly, with such slight differences, the wind stress drives the interior flow much like the pressure gradient. The scaled wind stress includes division by the local depth, so its effective strength diminishes in deeper water. Nevertheless, buoyancy advection in the bottom boundary layer reduces bottom stress, so the interior alongshelf flow continues to accelerate for many friction time scales. This could play an important role in the continuing acceleration and lack of a steady state in the recent numerical calculations of wind-driven upwelling by Lentz and Chapman (2004). In addition, if bottom stress remains small, then the onshore (offshore) flow that is required to balance the offshore (onshore) surface wind-driven Ekman transport cannot occur in the bottom boundary layer but must occur in the interior. This tendency is greater for larger Burger number, suggesting the following interesting scenario. For fixed stratification, S may be small over the shelf and, at the same time, much larger just seaward of the shelf edge because of the increase in bottom slope. Therefore, the onshore or offshore flow that balances the surface Ekman transport could be mostly in the bottom boundary layer over the shelf but almost entirely in the interior beyond the shelf edge. This implies a dramatic convergence or divergence into or out of the bottom boundary layer near the shelf edge. Hints of this behavior can be found in Allen et al. (1995).

6. Discussion and summary

We have presented an idealized model for the acceleration of a stratified flow over a sloping bottom, driven by a prescribed alongshelf pressure gradient. The model is constructed to elucidate the effects of buoyancy advection in the bottom boundary layer, while allowing both the interior and boundary layer flows to develop from an initially resting state. Both downwelling and upwelling pressure gradients are considered. The boundary layer model used for the downwelling case is essentially the same as that developed previously by Chapman and Lentz (1997) and Chapman (2002), but the boundary layer model used for the upwelling case is, to our knowledge, entirely new.

The most important result is that, for either a downwelling or an upwelling pressure gradient, thermal-wind shear within the boundary layer maintains a small bottom velocity, and hence weak bottom stress, that allows the interior flow to accelerate for a long time. The acceleration of the interior velocity increases dramatically with increasing stratification, as measured by the Burger number, S. This implies that an alongshelf pressure gradient could, in principle, generate very large alongshelf currents, especially if the stratification is strong. Or, conversely, a rather meager alongshelf pressure gradient could drive substantial alongshelf currents that could play a role in shelf dynamics. For example, it has been argued that an alongshelf sea level slope of 10^{-7} is needed to satisfy the alongshelf momentum balance in the Middle Atlantic Bight (e.g., Scott and Csanady 1976; Beardsley and Winant 1979). This is the same sea surface slope used to approximate $P_x = -0.02$ for the calculations shown above. For weak stratification, say $S = 0.1$, the interior velocity after 20 friction time scales is $u^i = 0.026$. The dimensional velocity is recovered by multiplying by the scale factor fh/α, which for $f = 10^{-4}$ s^{-1}, $h = 50$ m, and $\alpha = 0.001$ gives a velocity of 0.13 ms^{-1}, a reasonable value. However, if the stratification were stronger, say $S = 0.5$, then the steady-state interior velocity for the same situation would be $u^i = 0.78$ m s^{-1}, clearly unrealistically large. Similar results are obtained for an upwelling pressure gradient. Using the same parameter values as in the above examples, an upwelling pressure gradient applied for 20 friction time scales would produce an alongshelf velocity of $u^i = -0.2$ m s^{-1} for $S = 0.1$, and $u^i = -1.35$ m s^{-1} for $S = 0.5$. Thus, a reasonable alongshelf pressure gradient may be very effective at accelerating alongshelf flows while producing little bottom stress, even for moderately strong stratification.

The theoretical model results also suggest that, for either pressure gradient or wind forcing, low-frequency bottom stresses on stratified shelves are likely to be small owing to buoyancy advection in the bottom boundary layer. This is consistent with recent observations from several regions that indicate low-frequency bottom stress is weak relative to wind stress and/or alongshelf pressure gradients (Shearman and Lentz 2003; Werner et al. 2003; Lentz and Trowbridge 2001). Furthermore, mean pressure gradients on shelves are not measured directly but are typically inferred from dynamical balances because of the difficulty in determining the absolute position of pressure sensors or tide gauges relative to the geoid (e.g., Scott and Csanady 1976; Beardsley and Winant 1979). The results pre-

sented here suggest that bottom stress estimates based on depth-averaged currents or on current observations that are not close to the bottom may be inaccurate, particularly in regions where the Burger number is not small. Consequently, both the momentum balances and the inferred pressure gradients should be viewed with caution. Taken together, the present results raise the question of how important bottom stress is to low-frequency shelf dynamics, and they emphasize the need for direct bottom stress estimates based on turbulent covariances (e.g., Trowbridge 1998).

Numerous assumptions were made in developing the theoretical model; for example, the neglect of nonlinear advection in the momentum balances, geostrophic alongshelf flow even within the bottom boundary layer, particular bottom boundary layer structures for downwelling and upwelling, and horizontal interior isopycnals so the interior flow is barotropic. The agreement between the theoretical results and results from the two-dimensional numerical model, which does not make these simplifications, generally supports the use of these simplifying assumptions. However, care must be taken when applying the results. For example, the assumption that the interior isopycnals remain horizontal limits the applicability of the results to the region far enough offshore that divergences in the interior and boundary layer cross-shelf transports are small and do not tilt the interior isopycnals. For wind-driven upwelling or downwelling, the region of tilted isopycnals can extend far offshore because of the imposed Ekman transport in the surface boundary layer (e.g., Austin and Lentz 2002). Furthermore, a recent study suggests that the nonlinear terms in the momentum balances cannot be neglected in the region of tilting isopycnals (Lentz and Chapman 2004) and consequently the dynamics are more complicated than the present model suggests. On the other hand, the numerical model results indicate that pressure gradient forcing tilts the interior isopycnals only in a very narrow region near the coast. This is a direct consequence of the reduced bottom stress, which implies a weak cross-shelf transport in the bottom boundary layer and a weak return flow in the interior. Therefore, for flows driven by a pressure gradient, the theoretical model is relevant over almost the entire shelf, at least in the context of the two-dimensional numerical model. If so, the results suggest a need to reexamine coastal-trapped wave theory (e.g., Brink 1991), in which alongshelf pressure gradients provide a mechanism for transmitting momentum large distances along the shelf. The results presented here suggest that buoyancy shutdown should reduce the bottom drag on coastal trapped waves, allowing them to propagate much farther than predicted from a traditional friction time scale. The results also suggest that coastal trapped waves may be less effective at driving cross-shelf transports than the classical theory suggests.

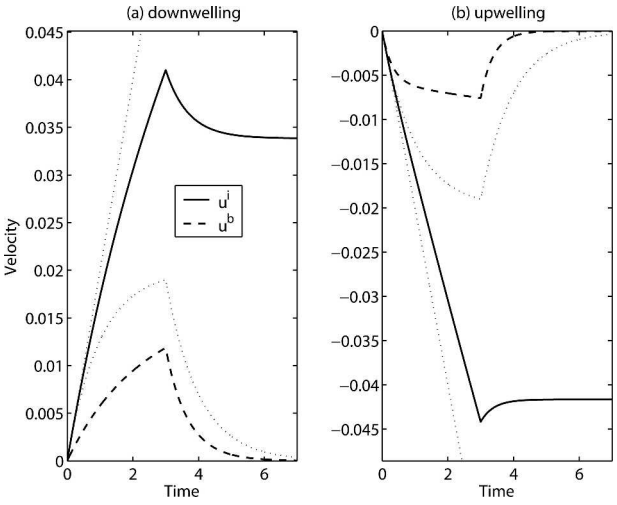

FIG. 12. Theoretical interior and bottom velocities in response to forcing of finite duration. A (a) downwelling or (b) upwelling pressure gradient is imposed until $t = 3$ and is then removed, with $S = 0.4$ and $P_x = \pm 0.02$ (and $r/fh = 0.0625$ for upwelling). Dotted straight lines show the response with no bottom friction. Dotted curves show the response with no stratification ($S = 0$).

Last, we have considered only constant forcing in the above calculations. However, the theoretical model is not restricted to this case. It is trivial to compute solutions for any specified forcing strength or duration. For example, suppose the pressure gradient acts for a finite duration and then vanishes. At this point, the interior flow stops accelerating and the entire water column slows until the bottom velocity vanishes; that is, $u^b \to 0$. Figure 12 shows both the downwelling and upwelling model responses to a pressure gradient that vanishes after three friction time scales. Thermal-wind shear in the boundary layer allows the interior velocity to remain in a nonzero steady state despite the lack of forcing because bottom stress vanishes once u^b decays to zero. There is then no mechanism to slow the interior flow. The final interior velocity, of course, depends on the velocity when the forcing ceases. These responses are qualitatively similar to the deceleration process studied by Chapman (2002), so they are not examined further here.

Acknowledgments. Funding was provided by the Division of Ocean Sciences of the National Science Foundation under Grant OCE-0241292. DCC also received some support from the Office of Naval Research under Grants N00014-00-1-0210 and N00014-02-1-0767.

REFERENCES

Allen, J. S., 1973: Upwelling and coastal jets in a continuously stratified ocean. *J. Phys. Oceanogr.,* **3,** 245–257.

——, and R. L. Smith, 1981: On the dynamics of wind-driven shelf currents. *Philos. Trans. Roy. Soc. London,* **302A,** 617–634.

——, and P. A. Newberger, 1998: On symmetric instabilities in oceanic bottom boundary layers. *J. Phys. Oceanogr.,* **28,** 1131–1151.

——, ——, and J. Federiuk, 1995: Upwelling circulation on the Oregon continental shelf. Part I: Response to idealized forcing. *J. Phys. Oceanogr.,* **25,** 1843–1866.

Austin, J. A., and S. J. Lentz, 2002: The inner shelf response to wind-driven upwelling and downwelling. *J. Phys. Oceanogr.,* **32,** 2171–2193.

Beardsley, R. C., and C. D. Winant, 1979: On the mean circulation in the Mid-Atlantic Bight. *J. Phys. Oceanogr.,* **9,** 612–619.

Brink, K. H., 1991: Coastal-trapped waves and wind-driven currents over the continental shelf. *Annu. Rev. Fluid Mech.,* **23,** 389–412.

Chapman, D. C., 2000: A numerical study of the adjustment of a narrow stratified current over a sloping bottom. *J. Phys. Oceanogr.,* **30,** 2927–2940.

——, 2002: Deceleration of a finite-width, stratified current over a sloping bottom: Frictional spindown or buoyancy shutdown? *J. Phys. Oceanogr.,* **32,** 336–352.

——, and S. J. Lentz, 1997: Adjustment of stratified flow over a sloping bottom. *J. Phys. Oceanogr.,* **27,** 340–356.

Gan, J., and J. S. Allen, 2002: A modeling study of shelf circulation off northern California in the region of the Coastal Ocean Dynamics Experiment: Response to relaxation of upwelling winds. *J. Geophys. Res.,* **107,** 3123, doi:10.1029/2000JC000768.

Garrett, C., P. MacCready, and P. Rhines, 1993: Boundary mixing and arrested Ekman layers: Rotating stratified flow near a sloping boundary. *Annu. Rev. Fluid Mech.,* **25,** 291–323.

Hamilton, P., and M. Rattray Jr., 1978: A numerical model of the depth-dependent, wind-driven upwelling circulation on a continental shelf. *J. Phys. Oceanogr.,* **8,** 437–457.

Hickey, B. M., 1984: The fluctuating longshore pressure gradient on the Pacific northwest shelf: A dynamical analysis. *J. Phys. Oceanogr.,* **14,** 276–293.

Lentz, S. J., 1994: Current dynamics over the northern California inner shelf. *J. Phys. Oceanogr.,* **24,** 2461–2478.

——, and C. D. Winant, 1986: Subinertial currents on the southern California shelf. *J. Phys. Oceanogr.,* **16,** 1737–1750.

——, and J. H. Trowbridge, 2001: A dynamical description of fall and winter mean current profiles over the northern California shelf. *J. Phys. Oceanogr.,* **31,** 914–931.

——, and D. C. Chapman, 2004: The importance of nonlinear cross-shelf momentum flux during wind-driven coastal upwelling. *J. Phys. Oceanogr.,* **34,** 2444–2457.

——, R. T. Guza, S. Elgar, F. Feddersen, and T. H. C. Herbers, 1999: Momentum balances on the North Carolina inner shelf. *J. Geophys. Res.,* **104,** 18 205–18 226.

MacCready, P., and P. B. Rhines, 1993: Slippery bottom boundary layers on a slope. *J. Phys. Oceanogr.,* **23,** 5–22.

Scott, J. T., and G. T. Csanady, 1976: Nearshore currents off Long Island. *J. Geophys. Res.,* **81,** 5401–5409.

Shearman, R. K., and S. J. Lentz, 2003: Dynamics of mean and subtidal flow on the New England shelf. *J. Geophys. Res.,* **108,** 3281, doi:10.1029/2002JC001417.

Smith, R. L., 1981. A comparison of the structure and variability of the flow field in three coastal upwelling regions: Oregon, Northwest Africa, and Peru. *Coastal Upwelling,* F. A. Richards, Ed., Amer. Geophys. Union, 107–118.

Trowbridge, J. H., 1998: On a technique for measurement of turbulent shear stress in the presence of surface waves. *J. Atmos. Oceanic Technol.,* **15,** 290–298.

——, and S. J. Lentz, 1991: Asymmetric behavior of an oceanic boundary layer above a sloping bottom. *J. Phys. Oceanogr.,* **21,** 1171–1185.

Weatherly, G. L., and P. J. Martin, 1978: On the structure and dynamics of the oceanic bottom boundary layer. *J. Phys. Oceanogr.,* **8,** 557–570.

Werner, S. R., R. C. Beardsley, and A. J. Williams III, 2003: Bottom friction and bed forms on the southern flank of Georges Bank. *J. Geophys. Res.,* **108,** 8004, doi:10.1029/2000JC000692.

Yankovsky, A. E., and R. W. Garvine, 1998: Subinertial dynamics on the inner New Jersey shelf during the upwelling season. *J. Phys. Oceanogr.,* **28,** 2444–2458.

Zamudio, L., and M. Lopez, 1994: On the effect of the alongshelf pressure gradient on numerical simulations over the northern California continental shelf. *J. Geophys. Res.,* **99,** 16 117–16 129.